Full-Wave Three-Dimensional EM Simulation of a Spherical Range to Examine and Optimise the Effectiveness of Mode Filtering Based Post Processing Techniques

S.F. Gregson[1, 2] Z. Tian[3]
[1] Next Phase Measurements LLC., LA, USA, stuart.gregson@npmeas.com
[2] Queen Mary University of London, London, UK, stuart.gregson@qmul.ac.uk
[3] National Physical Laboratory, Teddington, UK, zhengrong.tian@npl.co.uk

***Abstract*—This paper extends the authors' prior studies into the use of a very general digital twin of a spherical near-field antenna test system for the careful validation and further optimization of mode filtering-based post processing techniques for scattering suppression. This paper compares and contrasts various measurement configurations and several mode filtering strategies using the results thereof to make recommendations regarding the optimum acquisition strategy and preferred processing methodology. Results are presented and discussed with this paper being the first time that such an extensive and rigorous full-wave three-dimensional computational electromagnetic simulation campaign has been harnessed in this way. This has enabled cylindrical and spherical mode filtering-based scattering suppression techniques to be quantitatively compared, contrasted, and examined.**

***Index Terms*—mode filtering, CEM, spherical modes, cylindrical modes, polar measurement, equatorial measurement, digital twin.**

I. Introduction

For almost any indoor antenna measurement facility, irrespective of whether that system is a: planar, cylindrical, spherical near-field system, or compact antenna test range, room scattering is generally one of the most important terms within the range uncertainty budget [1]. This term tends to become especially significant when the range is required to operate outside its designated optimal working frequency band. A frequency domain, mode filtering-based measurement and post-processing-based technique has been successfully employed to reduce range reflections for over a decade now becoming an indispensable tool in the antenna measurement practitioner's arsenal. Although this technique has been extensively examined and validated experimentally [2, 3, 4] currently, comparatively little attention has, in the open literature, been devoted using full-wave three-dimensional computational electromagnetic (EM) simulations. This is primarily as a result of the very significant computational effort required to accomplish such a task. However, the flexibility and control that such an approach provides makes the effort worthwhile [2, 5]. This paper extends the authors previous studies involving the recent development of an electromagnetic model for cylindrical mode based far-field antenna scattering suppression [5]. That study is extended here to consider the significantly more complex case of the spherical range including polar and equatorial acquisition modes [2] as well as antenna displacements in a variety of directions. Thus, for the first time, a completely general EM model of the spherical measurement case was constructed and then employed to verify and optimize this crucial measurement and post-processing technique. The EM modelling technique is discussed with initial results presented which show very good agreement between the "ideal" far-field pattern and the perturbed far-field pattern once the scattering suppression processing has been applied. Furthermore, particular attention is devoted to establishing a criterion of how best to select the transformation center point required for optimal scattering suppression and a new best practice proposed which, rather crucially, simplifies the application of the post-processing and safeguards the quality of the results obtained.

II. Simulation Method

The three-dimensional computational electromagnetic (CEM) model presented in Fig. 1 comprised a circa 24 dBi, WR75 standard gain horn (SGH) which was used as the antenna under test (AUT). This medium gain aperture antenna had a rectangular aperture of size of 94 mm by 67 mm and a length of 200 mm. The AUT was initially positioned with its aperture located behind the origin of the rotation center, ($x = 0$, $y = 0$, $z = 0$), by 360 mm for an AUT z-translation test. As part of this study, the AUT was successively repositioned in both orientation and position so that additional acquisition modes could be examined. A perfect electric conducting (PEC) square plate with side of 200 mm was used as a scatterer and was positioned initially with its center located at (-2000, 0, 3000) mm and used to perturb the simulated antenna pattern measurement. The red dot shown at the left bottom of Fig. 1 represents the conceptual spherical measurement point at $\theta = 0°$, $\varphi = 0°$ for the case of an x-axis translated AUT. A more detailed description of the underlying model and simulation approach can be found presented in the open literature [5, 6] and hence here, only a summary is included.

Initially, the far-field of the AUT by itself, *i.e.* without the scatterer, was simulated using a conventional full-wave three-dimensional CEM simulation. This provided far-field results that could be used as a benchmark, *i.e.* truth model, against which other results could be compared for the purposes of this study. However, when the acquisition of the AUT was simulated in the spherical range, an entirely different approach was required.

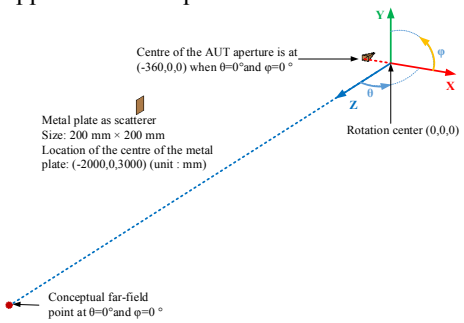

Fig. 1. Illustration of an full-wave three-dimensional electromagnetic model of a spherical antenna measurement for scattering suppression.

In a spherical antenna test system, one may consider that the AUT rotates around the rotation center in θ with an increment of Δθ and in φ with increment of Δφ where the order is unimportant. Thus, for cases where the scatterer is present and fixed in the chamber coordinate system, for each point within the spherical acquisition the relative position and orientation of the scatterer with respect to the AUT will be different resulting in every point within the simulated measurement requiring a different simulation. Thus, the measurement simulation can be seen to constitute a computationally very intensive, but parallelable, problem. The basic simulation task is especially well suited to the proprietary CST integral equation solver as it comprises principally metallic constituent parts set within a large expanse of vacuum. The solver process was fully automated by means of a dedicated macro. In this way, the far-field of each model at (θ_i, φ_i) was simulated. A second macro was then used to extract the far-field at the specific far-field point (θ_i, φ_i) from each corresponding model and then subsequently combined to form the complete simulated perturbed spherical pattern measurement data set of the AUT in the presence of the scatterer.

III. Simulated Measurement Results – Spherical Mode Based Post-Processing

Fig. 2 presents a comparison of the far-field copolar and cross-polar patterns of the AUT plotted on a true-view, *i.e.* θcosϕ, θsinϕ plotting system with the electric fields resolved onto a Ludwig III polarization basis for three cases plotted as a false colour checkerboard plot [2]. Fig. 2 (a) and (b) are plots of the AUT pattern with the scatterer perturbing the pattern. Fig. (c) and (d) present the simulated co- and cross-pol far-field pattern of the AUT alone, without the presence of any scatterer with this serving as a benchmark for the comparison. Fig. (e) and (f) present the far-field pattern with mode filtering scattering suppression data post process applied, from which it can be observed that the ripples have been effectively removed. In the simulated measurement the AUT was acquired in polar mode with the AUT having been displaced in the *z*-axis (which in this case was -360 mm). A *z*-axis translated AUT acquired in a polar pointing acquisition mode represents a very common measurement configuration for this form of scattering suppression measurement and was the primary motivation for adopting this setup [2]. The frequency with which this measurement modes is encountered is perhaps most likely an artefact of the typical ease with which an AUT may be offset from the origin of the measurement axis in this mode, with many measurements requiring either an upper horizontal linear slide or custom fixturing to place the AUT at the intersection of the θ- and ϕ-axes [2].

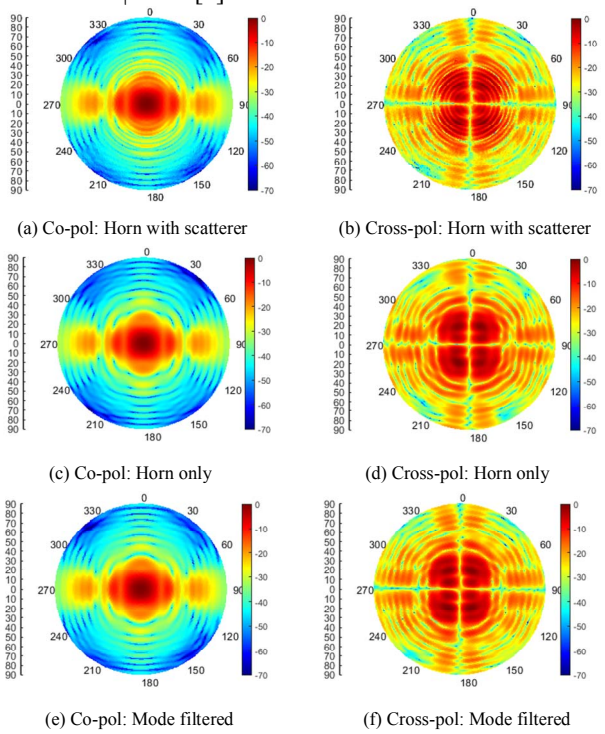

(a) Co-pol: Horn with scatterer (b) Cross-pol: Horn with scatterer

(c) Co-pol: Horn only (d) Cross-pol: Horn only

(e) Co-pol: Mode filtered (f) Cross-pol: Mode filtered

Fig. 2. Far-field pattern of the simulated measurement with and without the perturbing scatterer present and then with the mode filtering applied with a z-axis translated AUT.

A less common acquisition mode is to translate the AUT in the transverse direction, in either in the *x*- and/or *y*-axes. Results for this case can be seen presented in Fig. 3 below. Here, Fig. 3 (a) and (b) are plots of the AUT pattern with scatterer perturbing the measurement. Fig. (c) and (d) present the far-field pattern with mode filtering scattering suppression data post processing applied, from which it can be observed that the spurious ripples have been reduced. However, the suppression is not complete, and an additional *z*-axis translation was then also applied in an attempt to further improve the attenuation of the scattered signals. This can be seen presented in (e) and (f). From inspection of these figures it is clear that the transverse translation appears to be less effective than an equivalent *z*-axis translation and this requires further investigation. The transverse translation was required by virtue of the position of the AUT with

respect to the origin of the measurement coordinate system. However, as was noted within the prior work, [2, 3, 4, 5, 6] the optimum position of the AUT in the *z*-axis was a further 100 mm in the *z*-axis. This question is revisited below in Section IV however here, it is the reason that the patterns presented in Fig. 3 (e) and (f) were additionally translated in the *z*-axis.

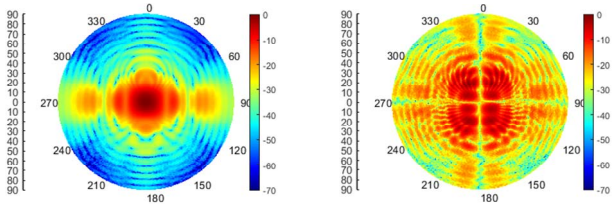

(a) Co-pol: Horn with scatterer

(b) Cross-pol: Horn with scatterer

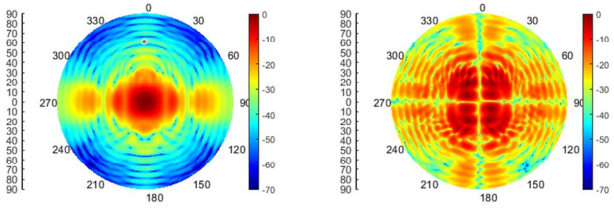

(c) Co-pol: Mode filtered with x-offset correction

(d) Cross-pol: Mode filtered with x-offset correction

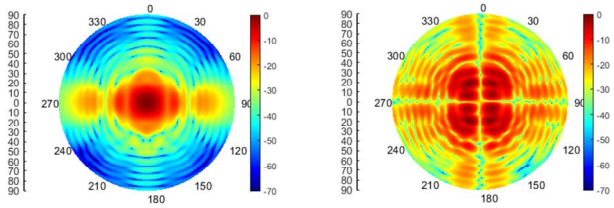

(e) Co-pol: Mode filtered with x- & z-offset correction

(f) Cross-pol: Mode filtered with x- & z-offset correction

Fig. 3. Far-field pattern of the simulated measurement with the perturbing scatterer present and then with the mode filtering of *x*-offset correction and *x*- & *z*-offset correction applied with an *x*-axis translated AUT.

During the course of the post-processing, it is required to compute the corresponding complex spherical mode coefficients (SMC). The power distribution of these spherical modes varies depending upon the location of the AUT with respect to the origin of the measurement coordinate system, *i.e.* the rotation center [2]. As a measure of the distribution of the mode spectra, the maximum polar mode index (N_{MAX}) that is required to contain 99.9995% of the total power can be computed, *i.e.* 6σ; as a function of AUT position. Fig 4. (a) presents a plot of the N_{MAX} as a function of position for three frequencies, 10 GHz, 13 GHz, and 15 GHz. From inspection of Fig. 4 (a) it can be seen that for all three frequencies, the N_{MAX} value is at a minimum when the rotation center is placed at the mid length of the AUT, *cf.* Fig. 4. (b). This is a phenomenon has been observed independently through measurements carried out in the actual spherical range that this simulation is a digital twin of [5, 6]. This is a significant observation as minimizing the band of spherical mode coefficients significantly eases the filtering process. This result will be further verified below through an equivalent analysis using a cylindrical-mode-based analysis in Section IV.

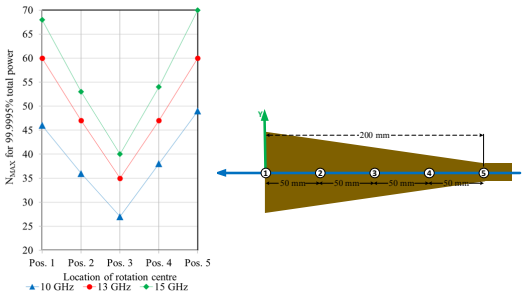

(a) N_{MAX} versus AUT positions (b) Illustratino of AUT positions

Fig. 4. Plot of N_{MAX} as a function of AUT position for the WR 75 SGH.

Now that the optimum position of AUT measurement configuration for the conventional polar mode acquisition has been established, the simulation was repeated for the alternative equatorial pointing acquisition. Here, the AUT's boresight direction was along the position *x*-axis as can be seen in Fig. 5 (a) and (b) below.

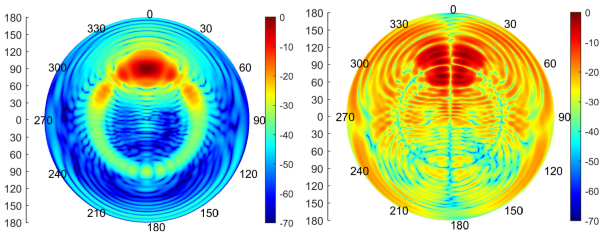

Fig. 5. Equatorial mode measurement, (a) EPhi left, (b) ETheta right.

Here, the far-field patterns have been presented in the same form as was used for Fig. 2 and Fig. 3. However, the interpretation of these results is complicated by virtue of the distortion in the patterns which is a consequence of the orientation of the AUT within the simulated spherical range. This difficulty may be resolved by rotating the AUT with respect to the plotting coordinate system [2]. This can be implemented rigorously, *i.e.* without recourse to polynomial interpolation by rotation of the spherical mode coefficients [7] with the results being presented in Fig. 6. As with the baseline polar-acquisition mode measurements, the mode filtering can be seen to be a highly effective technique for suppressing spurious scattering. However, in this case, the *z*-translation is far less effective than it was for the polar mode. The reason for this is that this corresponds to an *x*-axis translation in the polar mode case. Thus, for an equatorial mode measurement, the post-processing would be more effective if the antenna had instead been translated in the *x*-axis.

A subtlety exists in way the mode filtering can be applied in this case that is worthy of note. It is possible to apply the mode filtering to the SMCs either before the 90° rotation is applied, these results are presented in Fig. 6 (c) and (d), or after the rotation has been applied, and these results are presented in Fig. 6 (e) and (f). Although the windowing function would be the same in either case, the distribution of power amongst the respective SMCs would be different. In

this study, both cases were examined with very little difference being observed for the medium gain SGH that was examined herein. Although encouraging, this is clearly not exhaustive, and a further examination is planned. However, as this approach aligns most closely with the standard polar mode implementation, it was decided that the default would be to first rotate the SMCs and then to apply the windowing function.

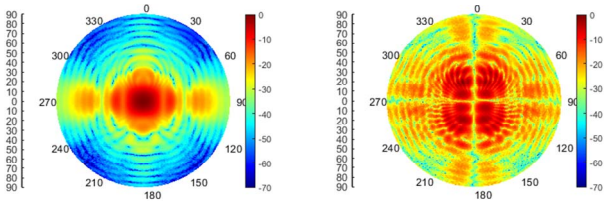

(a) Co-pol: Horn with scatterer

(b) Cross-pol: Horn with scatterer

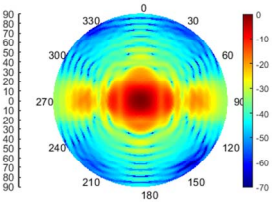

(c) Co-pol: Mode filtered (Rotation after filtering)

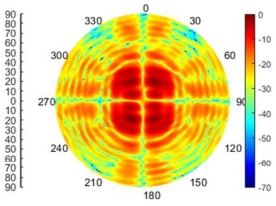

(d) Cross-pol: Mode filtered (Rotation after filtering)

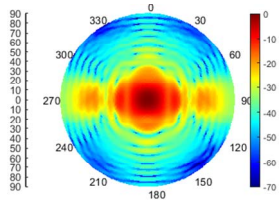

(e) Co-pol: Mode filtered (Rotation before filtering)

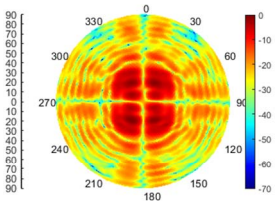

(f) Cross-pol: Mode filtered (Rotation before filtering)

Fig. 6. Far-field pattern of the simulated measurement with and without the mode filtering with a *z*-axis translated equatorial mounted AUT after the pattern has been rotated for the purposes of visualisation.

IV. Simulated Measurement Results – Cylindrical Mode Based Post-Processing

In the previous section a novel method for determining the optimum AUT translation was established that computed the spectrum of modes required to contain 6σ of the radiated power as a function of the position of the AUT. As the underlying mode basis should be unimportant, this analysis can be repeated using a cylindrical mode expansion of the antenna pattern, as opposed to a spherical mode expansion used above, and we would expect to observe the same effects. To verify this, for a far-field great-circle cut, the cylindrical mode spectrum was computed and the highest order cylindrical mode coefficient for which 99.9995% of the total power was contained was estimated. This was repeated for the 13 GHz case with the AUT being translated over the same *z*-axis 200 mm distance as was used in the preparation of Fig. 4 (a). This can be seen presented below in Fig. 7 (a). Importantly, as was seen with the spherical mode analysis, the analogues cylindrical mode analysis indicates the same position as being the optimum, *i.e.* being located at 100 mm back from the aperture of the pyramidal horn.

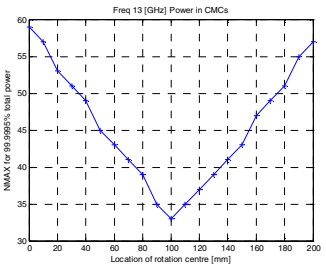

(a) N_{MAX} versus AUT position

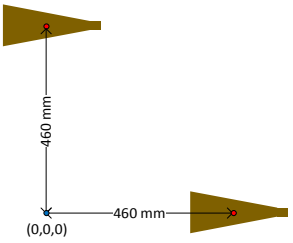

(b) Illustration of Position of WR75 SGH

Fig. 7. (a) Plot of N_{MAX} as a function of AUT position for the WR 75 SGH, (b) illustration of two positions of the AUT used during the cylindrical mode processing.

By way of a further check, the phase center of the horn was computed using a least squared functional fit across the main beam of the antenna, *i.e.* over the angular sector determined by the -15 dB beamwidth. This indicated that the phase center was positioned 28 mm behind the aperture of the WR75 SGH, which is sufficiently far from the position determined here as to suggest the two positions are different, and distinct from one another. However, there are a number of different definitions of phase center [8] and it is possible that the optimum position as determined within this study corresponds to some other definition. The utility of the position indicated by the mode distribution optimization is that it automatically guarantees the narrowest spectrum of modes which can be used for the mode filtering. The additional benefit is that this process can be embedded within the post-processing software enabling the user to automatically use the ideal position, and that no additional measurements are required to achieve this.

As a further verification of the scattering suppression technique, the far-field great circle cut from the simulations in the previous section was taken and used for far-field cylindrical mode based post-processing [2, 9]. The cylindrical mode coefficients for the unperturbed AUT can be found presented below in Fig. 8(a) which shows the AUT CMC spectrum before, red trace, and after mode filtering, blue trace, with a 0.15 m maximum radial extent (MRE) being used to determine the width of the mode filter function. This plot coloring convention was also employed within Fig. 8. (b) and (c) which, respectively, present equivalent plots for the perturbed antenna when translated in the *z*-axis and the *x*-axis where the position of the AUT is depicted above in Fig. 7(b). Here, in Fig. 8. (b) the *z*-translation has very effectively shifted the scattering to higher order CMCs that fall well outside of the spectrum of modes that are associated with solely the AUT, *cf.* Fig. 8. (a). This underpins the success of the mode filtering approach in this case. Conversely, the *x*-translation case depicted in Fig. 8. (c) it is evident that the modes associated with the scatterer are less well separated from those modes associated with the AUT than they were previously although the average level of the CMCs is higher at *circa* -40 dB, for $|n| > 50$. This is the

reason the reconstructed filtered far-field pattern is not as error free as would otherwise be the case.

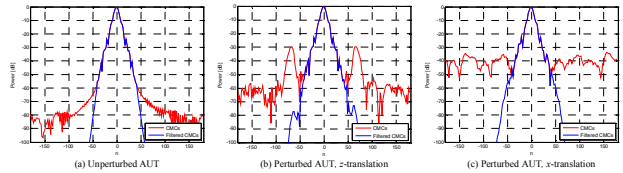

Fig. 8. (a) Plot of CMCs for unperturbed AUT, (b) plot of CMCs for perturbed AUT with z-translation, (c) plot of CMCs for perturbed AUT with x-translation.

The final part of this study comprised comparing the effectiveness of the spherical and cylindrical mode based post-processing techniques. One of the authors has conducted a similar comparison previously, however in contrast to this study, that was predicated on empirically derived data [10]. To this end, Fig. 9 (a) and (b) present respectively, the mode filtered far-field antenna patterns derived using cylindrical and spherical based mode processing for the cases where the AUT was displaced in the *z*-axis, and in the *x*-axis. Here, the side-lobes can be seen to have been attenuated in both spherical and cylindrically derived patterns with the high angular frequency ripple that was evident on the unprocessed patterns having been effectively suppressed. It is important to note that the spherical based processing utilizes the entire two-dimensional 4π steradian pattern whereas the cylindrical based processing uses merely a 2π radian cut. As such, one would anticipate that the spherical mode-based processing would be more effective and that is observed here, this is particularly evident from inspection of Fig. 9 (b) in the more demanding *x*-translation case. This effect has been observed empirically, *cf.* [11] and it is encouraging that it is also seen within the full-wave simulation. This is further illustrated by determining the RMS dB difference level between the two-post-processed patterns. For the *z*-translated case, the RMS dB difference level was -55.4 dB, whilst for the *x*-translated case, RMS dB difference level -37.19 indicating the greater difference between the two results for the *x*-translated case. Crucially however, this detailed study has confirmed that for both cylindrical and spherical based processing, for a polar-mode acquisition, the *z*-translation case is more effective when processing an antenna, such as the SGH considered herein, which has medium directivity.

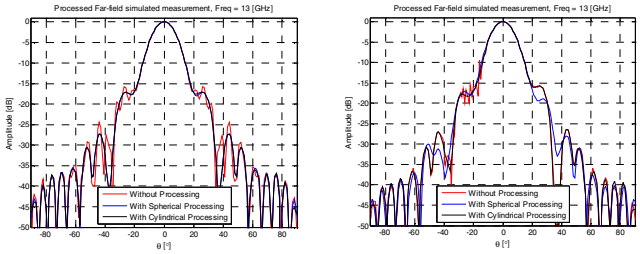

Fig. 9. Comparison plot of far-field pattern of AUT, perturbed AUT having been processed using CMC and SMC based scattering suppression where the AUT was displaced in the *z*-axis (a) left, and *x*-axis (b) right.

V. Summary and Conclusions

A very detailed, full-wave three-dimensional CEM model of a spherical antenna measurement system that can be used to investigate the impact of various error terms within the facility level error budget of a given spherical near- or far-field range has been developed and validated. This model has been used to recreate a conventional mode filtering-based scattering correction measurement whereupon similar phenomena have been observed in the CEM model as have been seen with actual range measurements. These include: the effects of scattering on a far-field pattern depend upon the AUT displacement with greater displacements resulting in larger angular frequency ripple, that the mode coefficients resulting from scattering are moved to higher order modes, with conversely AUT related modes being displaced towards lower order modes when the AUT is mathematically translated to the origin of the measurement co-ordinate system and lastly, that these mode-filtering based techniques are capable of very effectively suppressing scattering providing the magnitude of the displacement is sufficiently large, with translations in the boresight direction of the AUT being more effective. Crucially, and for the first time, a method for determining the optimum translation has been developed and verified using both spherical and cylindrical mode-based implementations.

Acknowledgment

This work was partially supported by the UK National Measurement System and the Department for Business, Energy, and Industrial Strategy.

References

[1] A.C. Newell, “Error Analysis Techniques for Planar Near-field Measurements”, IEEE Transactions on Antennas and Propagation, vol. AP-36, pp. 754-768, June 1988.

[2] C.G. Parini, S.F. Gregson, J. McCormick, D. Janse van Rensburg, “Theory and Practice of Modern Antenna Range Measurements”, IET Press, 2014, ISBN 978-1-84919-560-7.

[3] G.E. Hindman, A.C. Newell, “Reflection Suppression in a large spherical near-field range”, AMTA, Newport, RI, October. 2005.

[4] G.E. Hindman, A.C. Newell, “Reflection Suppression To Improve Anechoic Chamber Performance”, AMTA Europe, Munich, Germany, March 2006.

[5] S.F. Gregson, Z. Tian, “Verification of Generalized Far-Field Mode Filtering Based Reflection Suppression Through Computational Electromagnetic Simulation”, IEEE APS, Montreal, Canada, 2020.

[6] Z. Tian, S.F. Gregson, “Examination Of Spherical Antenna Far-Field Scattering Suppression Through Electromagnetic Simulation”, IET APC, Birmingham, UK, November, 2020.

[7] J.E. Hansen (ed.), “Spherical Near-Field Antenna Measurements”, The IET, UK, Peter Peregrinus Ltd., 1988. ISBN 0 86341 110.

[8] A.W. Rudge, K. Milne, A.D. Olver, P. Knight, “The Handbook of Antenna Design, Volume 1”, IET Press, 1982, ISBN 0-906048-82-6.

[9] S.F. Gregson, A.C. Newell, G.E. Hindman, “Reflection Suppression In Cylindrical Near-Field Antenna Measurement Systems – Cylindrical MARS”, AMTA, Salt Lake City, UT, November, 2009.

[10] S.F. Gregson, A.C. Newell, G.E. Hindman, M.J. Carey, “Comparison of Cylindrical and Spherical Mathematical Absorber Reflection Suppression”, LAPC, Loughbourough, UK, November, 2010.

[11] S.F. Gregson, A.C. Newell, G.E. Hindman, M.J. Carey, “Advances in Cylindrical Mathematical Absorber Reflection Suppression”, EuCAP, April, 2010, Barcelona, Spain.